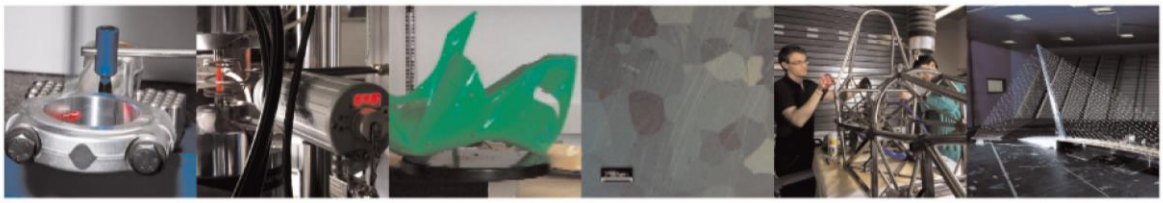

Understanding the effects of temporal waveform modulation of laser emission power in laser powder bed fusion: Part II - Experimental investigation

Caprio, L.; Demir, A. G.; Previtali, B.

This is a post-peer-review, pre-copyedit version of an article published in JOURNAL OF PHYSICS D. APPLIED PHYSICS. The final authenticated version is available online at: http://dx.doi.org/10.1088/1361-6463/ac98d1

DIPARTIMENTO DI MECCANICA ■ POLITECNICO DI MILANO
via G. La Masa, 1 ■ 20156 Milano ■ EMAIL (PEC): pecmecc@cert.polimi.it
http://www.mecc.polimi.it
Rev. 0

Understanding the effects of temporal waveform modulation of the laser emission power in Laser Powder Bed Fusion – Part 2: Experimental investigation

Leonardo Caprio[1]*, leonardo.caprio@polimi.it,

Ali Gökhan Demir[1], aligokhan.demir@polimi.it

Barbara Previtali[1], barbara.previtali@polimi.it

[1]Department of Mechanical Engineering, Politecnico di Milano, Via La Masa 1, 20156 Milan, Italy

*Corresponding author

Understanding the effects of temporal waveform modulation of the laser emission power in Laser Powder Bed Fusion – Part 2: Experimental investigation

Leonardo Caprio[1]*, Ali Gökhan Demir[1], Barbara Previtali[1]

[1]Department of Mechanical Engineering, Politecnico di Milano, Via La Masa 1, 20156 Milan, Italy

* Corresponding author

Abstract

The Laser Powder Bed Fusion (LPBF) process has been historically operating with high brilliance fiber laser sources with Continuous Wave (CW) emission. Nonetheless, temporal waveform modulation of the laser emission power at high frequency levels can provide a means to enhance the deposition process by modifying the melt dynamics and solidification mechanisms. In order to disclose the effect of different waveform shapes and their parameters, an experimental study using an open LPBF system was conducted. This work configures as the second part of an investigation on this topic with the aim of validating the analytical model proposed in the first part of this work. The LPBF system developed enabled to program the power emission profiles during single track depositions. Four different waveform shapes were tested (namely Square Wave, Ramp Up, Ramp Down and Triangle Wave) at different levels of waveform amplitude (ΔP=200-400 W) and different frequencies (f_w= 2 – 4 – 6 – 8 kHz) during the single track deposition of stainless steel AISI316L. High speed imaging acquisitions allowed to disclose the melt dynamics and identify the melt oscillation frequency. Larger waveform amplitudes and waveforms with sudden variations of the emission power generated melt ejections and process instabilities. Stable conditions could be identified when employing Ramp Up and Triangle waveforms with ΔP=200. Melt surface oscillation frequency corresponded to the values imposed via the modulation of the laser emission power thus validating the analytical model of Part I which correlated the melt surface temperature to the recoil pressure induced over the molten pool. Optical microscopy images and metallographic cross-sections confirmed the high speed video observations. 3D reconstructions of the depositions via focus variation microscopy allowed to determine the build rates and roughness of the single tracks. Build rates obtained in stable deposition conditions

with waveform modulation are analogous to values obtainable with CW emission and beneficial effects over the roughness were reported.

Keywords:

Additive Manufacturing, Laser Powder Bed Fusion; Waveform; Modulation; Laser material processing; High speed imaging

List of Symbols

Symbol	Name	Units
BR	Build rate	mm^3/s
d_0	Beam waist diameter	µm
f_{acq}	High speed camera acquisition frequency	Hz
$f_{osc,meas}$	Measured oscillation frequency of the melt pool	Hz
$f_{osc,theo}$	Theorically predicted oscillation frequency of the melt pool	Hz
FOV	Field of view	pixel × pixel / mm × mm
f_w	Waveform frequency	Hz
l	Single track length	mm
l_t	Layer thickness	µm
m	Number of replicates	-
M^2	Beam quality factor	-
P_{avg}	Average laser emission power	W
P_{bk}	Background power of laser emission	W
P_{max}	Maximum emission power	W
P_{pk}	Peak power of laser emission	W
SR	Spatial resolution	µm/pixel
t_{exp}	Exposure time of CMOS camera	µs
t_{fall}	Laser fall time	µs
$t_{illumination}$	Exposure time of illumination light	µs
t_{off}	Laser off period	µs
t_{on}	Exposure time	µs
t_{rise}	Laser rise time	µs
t_{tot}	Waveform period	µs
V	Volume of deposited material	mm^3
δ	Duty cycle	Non-dimensional
ΔP	Waveform amplitude	W
Λ_{obs}	Observation wavelength	nm
$\Lambda_{process}$	Laser emission wavelength	nm
α	Thermal diffusivity	m^2/s
λ	Spatial wavelength of the process	µm

1 Introduction

The development of the Laser Powder Bed Fusion (LPBF) process and its widespread adoption on behalf of the industrial community has progressed at an exceptional rate in the past years as demonstrated in the review by Schmidt *et al.*[1]. Advancements in the architecture of laser sources, from systems with CO_2 or Nd:YAG active mediums to high brightness Yb:glass fiber lasers, enabled the transition to complete melting and solidification of the feedstock material yielding fully dense material [2]. Nonetheless, major challenges reside in the process productivity as well as the microstructural control obtainable. The thermo-fluid dynamic aspects of the melt pool generated by the laser material interaction are of fundamental importance in ensuring a stable and fruitful deposition process. Thus the strong interest of the scientific community in investigating different solutions in terms of laser beams and their parameters to maximise the process efficiency

Since the introduction of the fiber laser in the Additive Manufacturing (AM) market in the early 2000s, these laser sources have been consolidated in industrial LPBF systems. As reviewed by Caprio *et al.* [3] and Gusarov *et al.* [4] the majority of system manufacturers employs Gaussian shaped beams with continuous wave emission of the laser to process the metallic powder. The process resolution and performance are intrinsically connected to the molten pool characteristics generated by the laser-material interaction when the beam is scanned at elevated velocities over the powder bed. Industrial solutions currently provided have been concentration on the use of multiple single-mode laser beams over the same scanning area to improve process productivity.

Still, it has been shown that the use of spatial and temporal beam shaping techniques may be beneficial for the process outcome. With regards to spatial modulation of the beam shape, Roehling *et al.* [5,6] showed the potential of elliptical beams to obtain a greater microstructural control over the LPBF process. Other investigations were conducted employing spatial beam shaping as solutions to crack formation or to enhance the processability and productivity of metals [7–9]. The combined effect of single-mode laser beams is typically employed to maximise the productivity of LPBF components as shown by Heeling and Wegener although Zhang *et al.* demonstrated their use to generate periodic structures during the deposition[10,11]. Futuristic work regarding the use of an optically

addressable light valve to directly obtain a projection of a layer (or part of it) instead of scanning the process light with galvanometric mirrors was reported by Matthews *et al.* for the processing of tin[12].

Alternatively, attempts at enhancing the LPBF process have been researched in the use of pulsed wave (PW) laser emission to optimize. Early work by Mumtaz and Hopkinson [13] showed that different shapes of the emission profile generated by a flash pumped Nd:Yag laser source in the millisecond regime may allow on the roughness profiles of thin walled structures. Caprio *et al.* through high frequency modulation showed that pulsed emission in the μs regime yields a finer molten pool which improves the process resolution although it has a detrimental effect on the volumetric deposition rate[14]. Successive work by Demir *et al.* indicates that modulated emission may be employed to avoid the formation of overheating region during the LPBF process[15]. Evidence that temporal modulation with respect to continuous wave (CW) emission has an impact on mechanical properties of materials has been reported by Biffi *et al.* [16] for AlSi10Mg and by Wilson-Heid *et al.* [17] for Ti6Al4V. Xiao *et al*. [18,19] have showed that for powder blown directed energy deposition of IN718, modulation of the power emission in the millisecond range can have a positive effect in improving both elongation and yield strength due to the reduced formation of Laves phase. Recent work by Baraldo *et al.* [20] also shows how conventional laser power modulation may be employed to build a control architecture.

Fiber laser systems typically employed in industrial LPBF machines enable the fast modulation of the emission with negligible rise and fall times ($\leq 5\mu s$ in changing between zero and the peak level of emission power). This technological aspect enables user to regulate the laser emission through arbitrary waveforms which may be optimised to enhance the Laser Powder Bed Fusion process. Applications of power temporal waveform modulation as a process enhancement tools may be found in other laser material processing fields. For instance, Neto *et al.* [21] experimented different waveforms and square waves to obtain a finer grain structure to improve the mechanical properties of the weld bead. On the other hand, Temmler *et al.* employed sinusoidal power variations for surface structuring applications of IN718 alloy[22]. Further works in the welding field, show the applicability of temporal waveforms during the laser welding of AZ31 Mg alloy and hybrid MIG-laser welding of pure copper [23,24].

Observing the current industrial and scientific panorama, the use of temporally modulated laser emission profiles emerges as a possibility to enhance the LPBF process and requires further attention. The present work configures as the second part of a preliminary investigation on the effect of different waveforms during the single track LPBF deposition of AISI316L. The overall logical scheme reporting the structure of the research conducted is shown in Figure 1.

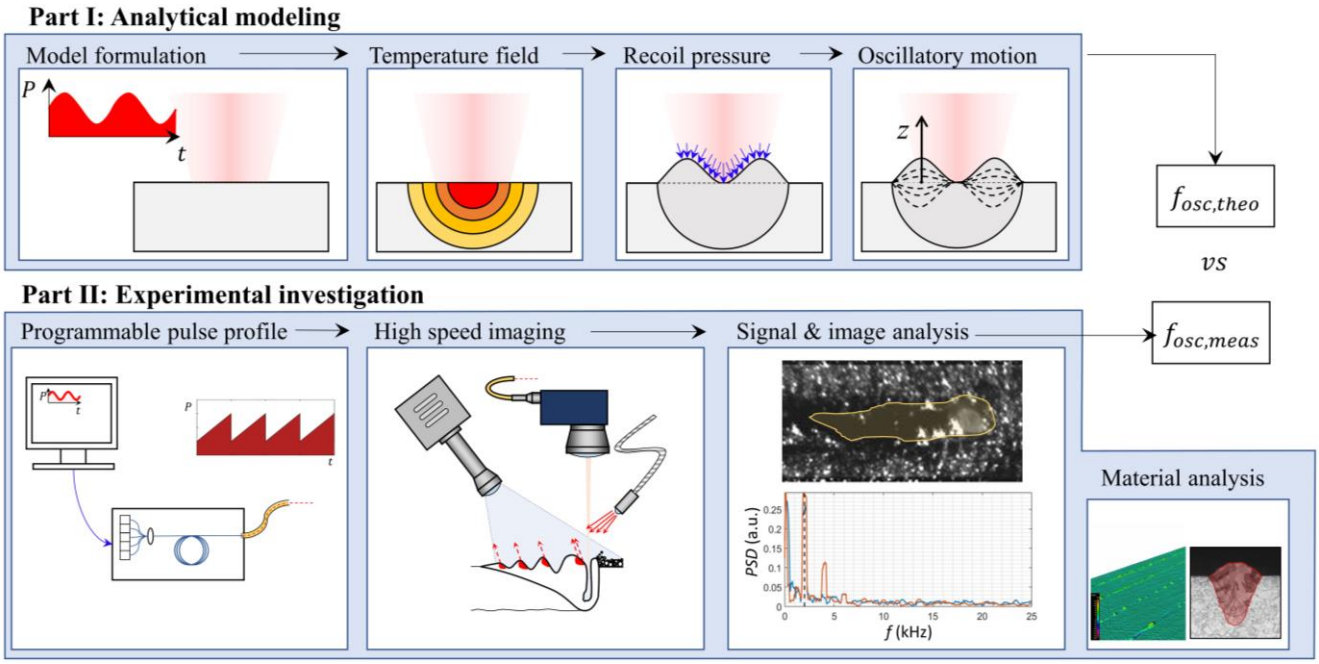

Figure 1. Overall structure of the research conducted to investigate the effect of temporally modulated beams during the LPBF process

The first part, presented in a separate publication, reports an analytical model to predict the effect of power modulation over the melt dynamics. The model allows to estimate the temperature field generated by a time-varying power input during the LPBF process. Given the temperature distribution it is possible to estimate the recoil pressure induced over the melt and consequently the oscillatory motion induced characterised by a theoretical oscillation frequency ($f_{osc,theo}$). This manuscript, which configures as the second part of the research, reports the results of an experimental investigation conducted to validate the model predictions and provide an insight over the potential of waveform modulation as an enhancement tool for the LPBF process. An in-house made flexible LPBF system with a laser source with programmable profiles was employed to obtain single track depositions with the use of different waveforms. High speed imaging acquisitions with external illumination were

conducted to observe the effect over the molten pool dynamics and characterize surface melt oscillations by measuring the melt oscillation frequency ($f_{osc,meas}$). Focus variation microscopy enabled the three-dimensional reconstruction in order to assess volumetric deposition and roughness of the single tracks. Results provide the first empirical indications with regards to promising waveform shapes and their parameters as an improvement tool of the LPBF process.

2 Materials and methods

2.1 LPBF system

An open prototypal Laser Powder Bed Fusion system was used for the present investigation since it enabled the integration of high speed imaging equipment with the laser system and process chain. The system has been presented in detail in previous publications where its open architecture has enabled faster process development due to its flexibility in integrating different hardware components or laser systems [15,25,26]. A rubber recoater is put in motion by two stepper motors to deliver the powder feedstock over the process area whilst a z-axis enables the user to control the layer thickness. The powder delivery system and motion are controlled by an in-house developed Labview program. (National Instruments, Austin, TX, USA). Localised inertization of the laser-material interaction area was achieved via a gas nozzle blowing 99.999% pure Ar gas at a pressure of 3 bar delivered through a 6 mm diameter tube. Inert gas flow can affect significantly build quality as reported by Ferrar *et al.*[27]. From a phenomenological perspective, gas flow rate can impact on both the thermal and fluid dynamic aspects as observed by Zhao *et al.* during the welding process [28]. Hence, modifications to plasma plume induced by different inertization conditions can significantly modify the deposition conditions as observed by Chen *et al.*[29]. In order to maintain the experimental conditions under control, the inertization procedure was maintained consistent throughout the baseplate and in the different experiments conducted.

2.2 Laser system and process chain

A single mode 1000 W fiber laser was employed as process light during the current investigation (nLight Alta, nLight, Vancouver, WA, USA). The emission wavelength ($\lambda_{process}$) corresponded to 1078 nm. The laser beam was

collimated prior to entering a scanner head (Smart Scan, Smart Move GmbH, Garching bei München, Germany) which allowed to deflect it on the work area. The deflected beam was focused onto the workplane by means of a 420 mm F-Theta lens thus achieving a theoretical beam waist diameter (d_0) of 78µm. The nLight Alta 1kW laser source enables the programming of laser emission waveforms through the graphical user interface of the laser system. The *a priori* programming of the laser emission enables a fast control of the power profiles with rise (t_{rise}) and fall times (t_{fall}) lower than 5 µs thus providing a high flexibility in the choice of temporal waveforms. Moreover, the laser source permits the programming of laser emission profiles with modulation between non-zero values.

An EC1000 controller card was employed to coordinate the laser emission with its trajectory on the work plane,. A 5 V digital signal from the controller unit was employed to trigger the laser emission with the desired waveform whilst controlling the motion of the galvanometric mirrors through the XY2-100 protocol. Scan Master Designer software was used to define the scan paths and manage the digital outputs to the laser system (Cambridge Technologies, Bedford, MA). The overall specifications of the laser system are reported in Table 1.

Table 1. Specifications of the laser system and optical process chain

Parameter	Value
Maximum emission power, P_{max}	1000 W
Beam quality factor, M^2	1.19
Emission wavelength, $\Lambda_{process}$ (nm)	1078
Rise and fall time $t_{rise/fall}$	< 5 µs
Beam waist diameter, d_0 (µm)	78

2.3 Materials

The baseplate for the single track depositions was a 12 mm thick AISI316L stainless steel plate machined to fit onto the prototypal LPBF platform. Gas atomized of the same material with a granulometry comprised between 15 and 45 µm was employed as feedstock material. In Table 2 the chemical composition of the AISI316L powder is reported.

Table 2. Chemical composition of the AISI316L powder

Element	C	Si	Mn	P	S	Cr	Mo	Ni	Co	Ti	Fe
wt (%)	0.02	0.52	1.50	0.010	0.007	17.3	2.46	11.4	-	-	Bal.

2.4 High speed imaging equipment

High speed videography of the LPBF process were obtained by using a fast acquisition CMOS camera (Fastcam Mini AX200, Photron, Tokyo, Japan) coupled with an external illumination light (Cavilux HF, Cavitar, Tampere, Finland). The secondary light is pulsed non-coherent laser beam (wavelength Λ_{obs}=640 nm) which is employed to dominate the emission from the process and disclose the actual molten pool geometry. In accordance with the design cues for a monitoring set up defined by Mazzoleni *et al.* [30], the acquisition frequency of the illumination laser was synchronised with the acquisition rate of the high speed camera, whilst the exposure time of the CMOS sensor (t_{exp}) was regulated to slightly exceed the pulse duration of the Cavilux HF emission ($t_{illumination}$). In order to observe the laser material interaction and molten pool with sufficient spatial and temporal resolution, the field of view (*FOV*) was set to 1024 pixels x 96 pixels allowing to achieve a frame acquisition frequency f_{acq} of 50 kHz. The imaging unit was set to obtain a high magnification which yielded a spatial resolution (*SR*) of 5.5 µm/pixel on the focal plane. The details of the imaging set up are reported in Table 3.

Table 3. Specifications of the high speed imaging set up

Parameter	**Value**
Observation wavelength, Λ_{obs}	640 nm
Exposure time, t_{exp}	0.49 µs
Illumination time, $t_{illumination}$	0.39 µs
Spatial resolution, *SR*	5.5 µm/pixel
Field of View, *FOV*	1024 pixels × 96 pixels 5.632 mm × 0.528 mm
Acquisition frequency, f_{acq}	50 kHz

The high speed video acquisitions could be employed to measure the melt pool oscillation frequency according to the methodology developed by Caprio *et al.* [25,31]. The frames acquired were analysed by identifying a region of interest (ROI) just behind the laser-material interaction position and quantifying the specular reflections of the secondary illumination light in such region. The specular reflections were measured through the summation of the pixel intensities to yield a time-varying intensity indicator $I_{sum,ROI}$. Finally, analysing this time-varying signal in

the frequency domain and employing Thompson's multi-taper method to estimate the Power Spectral Density of the signal it was possible to identify the peak which corresponded to the main oscillation frequency of the melt f_{melt}. The overall configuration of the experimental set up showing both the LPBF system and the high speed videography equipment is reported in Figure 2.

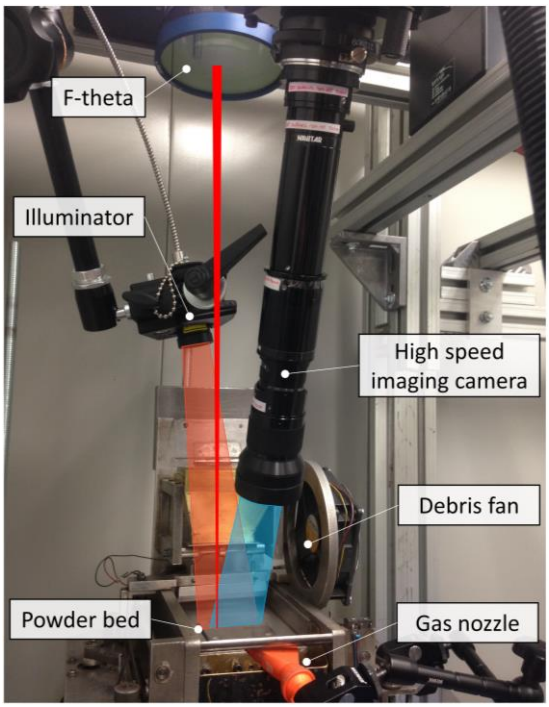

Figure 2. Experimental set up consisting of prototypal powder bed, laser system and high speed imaging equipment

2.5 Experimental Plan

The aim of the present work is to provide a preliminary investigation regarding the effect of different temporal waveforms during the LPBF process. Hence, the experimental campaign was designed to explore the impact of different temporal emission profiles on the melt motion via the high speed videos and comparing such with the predictions reported in part I: Analytical modelling of the present work. The experiments were designed to provide a constant energy per scan track. Hence, the laser scanning speed (v) was fixed at 300 mm/s and the average emission power (P_{avg}) at 200W. Such conditions, in the case of continuous wave emission of the laser power (i.e. without temporal modulation) were shown to provide a stable process for the realisation of thin walled specimens during preliminary experiments (which are not reported for brevity in the present manuscript). Hence, the CW

emission could was taken as reference condition of a stable process. Four different wave shapes were investigated, namely Square Wave (SQW), Triangle Wave (TRW), Ramp Up Wave (RUW) and Ramp Down Wave (RDW). Square Wave with a duty cycle level of 50% was considered representative of typical processing conditions when employing modulated emission as investigated in past research by Caprio *et al.* [3]. On the other hand, the other waveforms exhibited shapes with gradual increases in laser emission power from the background to the peak level (corresponding to Ramp Up), gradual decreases (Ramp Down) and both a gradual increase and decrease (i.e. Triangle Wave emission). In Figure 3, their schematic representation is reported.

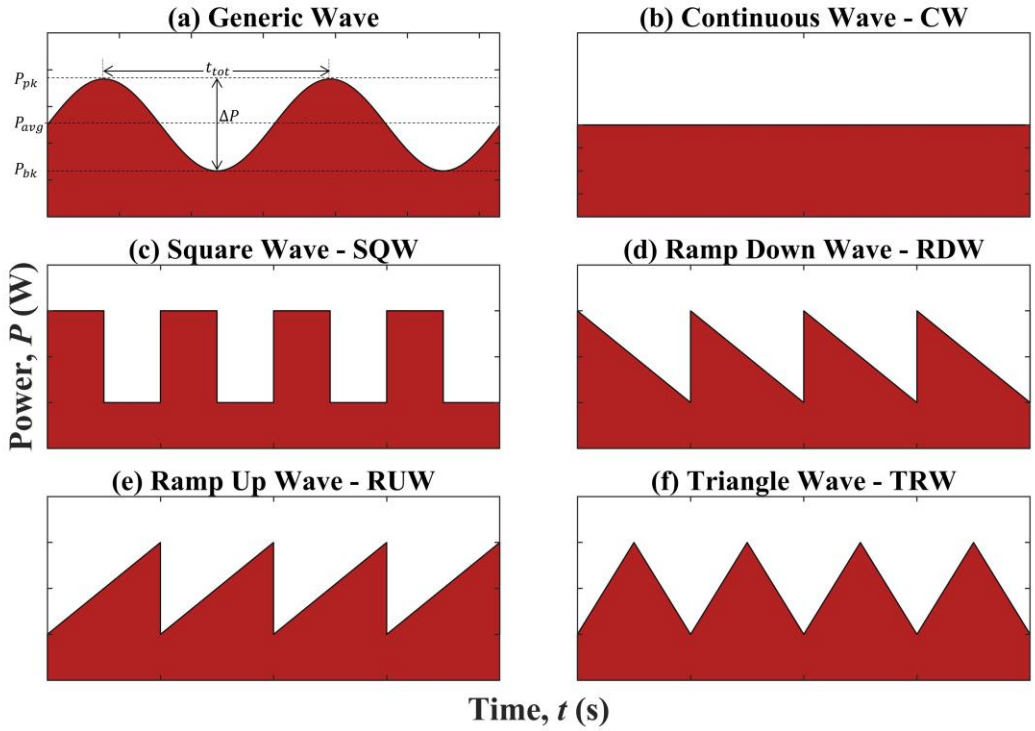

Figure 3. (a) Schematisation of parameters for a generic waveform, (b) Continuous Wave CW emission, (c) Square Wave *SQW*, (d) Ramp Down Wave *RDW*, (e) Ramp Up Wave *RUW* and (f) Triangle Wave *TRW*

Four different levels of wave frequency were associated to the present investigation (f_w=2-4-6-8 kHz) such that the spatial wavelength of the waveform did not exceed twice the waist diameter of the laser beam (λ_w correspondingly ranging from 150 to 36 µm). Two levels of amplitude ΔP were associated to the waveforms such that power oscillated between P_{bk}=100 and P_{pk}=300 W and between P_{bk}=0 and P_{pk}=400 W (i.e. ΔP=200-400 W). The emission profiles were measured a fast photodiode prior to the experimental study. Linear paths of 20 mm length with associated the different experimental conditions were scanned over a 50 µm thick powder bed with

localised Ar gas inertization (as done in previous investigations by Caprio *et al.*) [31]. Details of the experimental campaign are reported in Table 4. The conditions tested empirically correspond to the simulations realised for part I: Analytical modelling. Each experimental condition was replicated twice (m=2) in order to assess the main effects of the waveforms parameters whilst considering the wide range of experimental design. This number of replicates was considered sufficient to discern the main effects within this first investigation on the topic given past experience of the authors and in accordance with literature which conducted investigations also with a single replicates)[32,33].

Table 4. Fixed and variable factors of experimental campaign

Fixed factors	
Shielding gas	Argon
Material	AISI316L
Average power, P_{avg} (W)	200
Scan speed, v (mm/s)	300
Layer thickness, l_t (µm)	50
Replicates, m	2
Variable factors	
Temporal waveforms	Square Wave – Triangle Wave Ramp Up – Ramp Down
Wave frequency, f_w (kHz)	2 – 4 – 6 – 8
Wave Amplitude, ΔP (W)	200 – 400

2.6 Characterisation equipment

Optical microscopy was employed for qualitative evaluation of the single track depositions. A focus variation microscope (Infinite Focus, Alicona, Graz, Austria) was employed to obtain three-dimensional reconstructions of all the single tracks deposited. Acquisitions with 5X magnification had a vertical resolution of 0.5 µm and lateral resolution of 7 µm. By measuring the volume of deposited material V it was possible to determine the build rate according to the following relation:

$$BR = \frac{V \cdot v}{l} \tag{1}$$

where l is the length of the single track. In the case material was ejected from the deposition region this corresponded to negative values of build rate. Average surface roughness of the top profile of the single track depositions could also be measured using the focus variation microscopy acquisitions employing a cut-off wavelength of 800 µm. Measurement variability was assessed during preliminary acquisitions on representative samples and was thus assessed as orders of magnitude smaller with respect to the measurement values. For such reason measurement error bars are not reported in the results section but rather only the individual measurement values.

In order to disclose the sub-surface geometry of the melt, the single tracks were cut transversally to conduct metallographic analysis. After mechanical grinding and polishing, the cross-sectional geometry of the melt was exposed by means of a chemical etchant which consisted in a solution with 1 part of nitric acid 65% concentration, 1 part chloridic acid 37% concentration and 1 part distilled water.

In order to verify the effective temporal profile of the laser emission, the waveform emission in the different conditions was acquired by means of an InGaAs photodiode (FGA10, Thorlabs, Newton, NJ, USA). The measurement procedure is described in detail by Caprio *et al.* [14].

3 Results

3.1 Verification of the laser emission profiles

The emission profile in the different conditions tested throughout the experimental plan are reported in Figure 4. The measured pulse profiles realised with the laser system reflect well the theoretical waveforms programmed. Only a low power cut-off below 90 W occurs (which roughly corresponding to 10% of the nominal emission level of the laser system) slightly distorting the waveforms with amplitude ΔP=400 W and with rising or decaying temporal profiles (i.e. Ramp Down, Ramp Up and Triangle Wave).

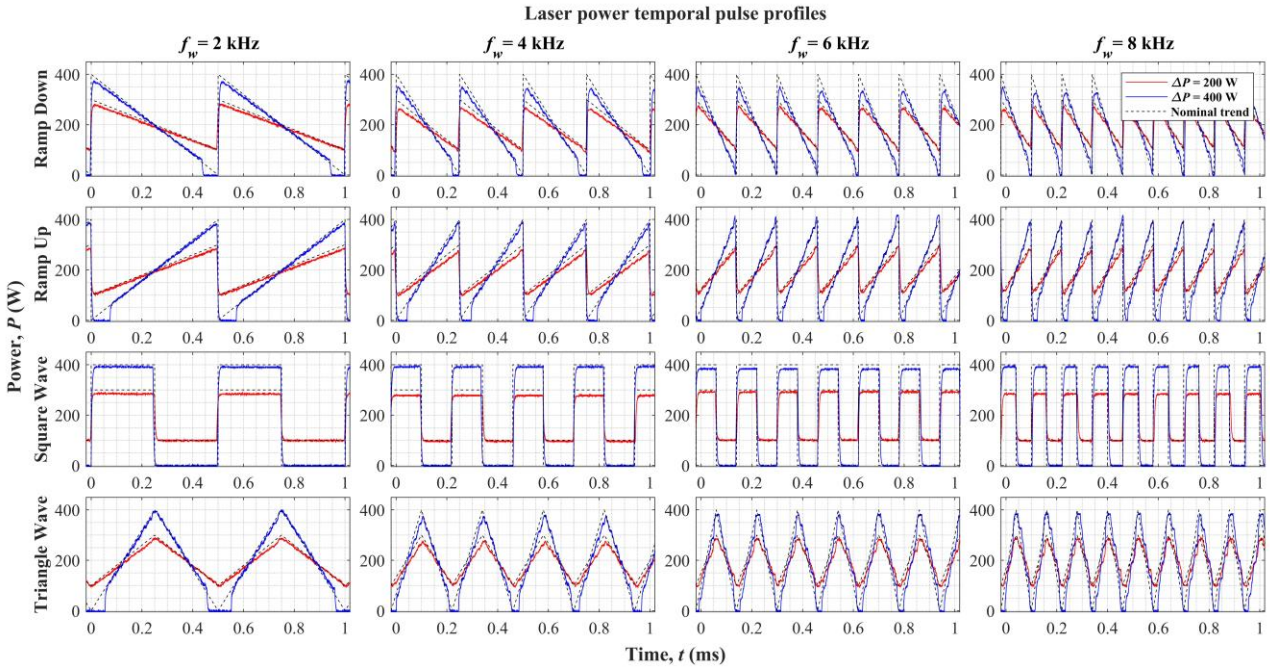

Figure 4. Temporal profile of the laser power in the different waveform employed during the experimental plan. Nominal trend in black dashed lines and measured temporal profile for ΔP=200 W in red and for ΔP=400 W in blue.

3.2 High speed imaging and melt oscillation frequency measurements

The interaction between the laser beam and the metallic powder was captured by means of high speed videography and still frames of the acquisitions are reported in Figure 5 for deposition at fixed level of waveform frequency (f_w=2 kHz) in the different variations of the process parameters (the full recordings of a representative condition are shown in Supplementary video n°3). The molten pool contours shown in Figure 5 allow to qualitatively identify the molten pool geometry at the specific instant reported. On the other hand, the melt geometry is more easily detectable observing dynamically the high speed imaging videos reported in Supplementary video n°3. The melt geometry is easily identifiable in the illuminated frames acquired since it appears to be in motion with respect to the static background and it is characterised by a dark black appearance with occasional bright reflections over the melt surface. More advanced analysis techniques to identify and measure the molten pool geometry such as those presented by Caprio *et al.* in previous work however could not exploited due to the significant challenges posed by the considerable melt ejections[31].

Observing the high speed acquisitions, it can be clearly noticed that the higher level of waveform amplitude (ΔP=400 W) generates greater melt ejections with respect to the case with ΔP=200 W. This aspect confirms the estimates reported in Part I: Analytical modelling which indicated that higher values of recoil pressure would be instantaneously induced over the melt due to the higher peak temperatures achieved at greater levels of waveform amplitude. Concurrently, the conditions with greater melt ejections correspond to situations where the molten pool length results being shorter of hundreds of microns. This phenomenon is consistent with the loss of material which appears more significantly in the case of waveforms with sudden increases in emission power (i.e. Ramp Down and Square Wave). Moreover, lower waveform amplitude conditions (ΔP=200 W), beyond exhibiting fewer ejections, also report a more stable and constant molten pool geometry.

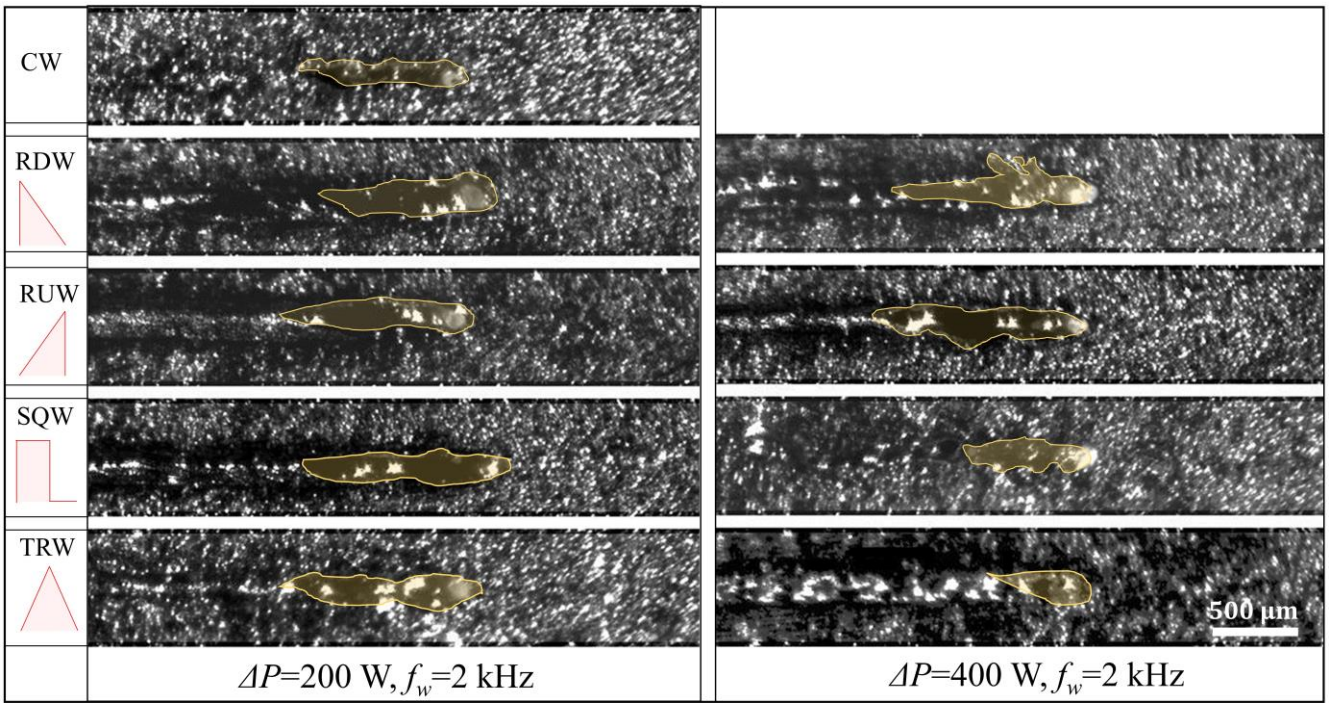

Figure 5. Frame from the high speed imaging acquisitions at a fixed level of waveform frequency f_w at different levels in terms of waveform and wave amplitude ΔP. The reader is also referred to Supplementary Video n°3. Molten pool contours highlighted manually in yellow.

In terms of waveform shapes, a stable melt formation may be observed in the case of the Ramp Up and Triangle Wave profiles. Contrarily to observations by Mumtaz and Hopkinson [13] during the deposition with a ms-pulsed Nd:YAG source, Ramp Down pulse waveform appear to have a detrimental effect during single-track depositions. The reason for such effects appears to be related to the sudden increase in laser power emission over on the molten liquid which generates an immediate rise in recoil pressure and may cause melt ejections. The principles of such physical mechanism were described by Semak *et al.* [34] when defining the onset of keyhole formation. Analogously, melt instability effects may be denoted when the Square Wave is employed. This aspect is once again in accordance with the predictions of the analytical model which identified peaks in terms of recoil pressure whenever a fast variation in terms of emission power occurs. The high speed imaging acquisition Triangle Wave and Ramp Up profiles at ΔP=200 W, on the other hand, show a stable melt formation which is symptomatic of a consistent deposition process.

The effect of the waveform frequency is more difficult to be observed qualitatively from the high speed videography. Thus in order to characterize the effect of the waveform frequency over the melt dynamics, the melt

surface oscillations where characterised by measuring the reflections of the illumination light. The time-varying indicator of the intensity of the surface reflections was analysed in the frequency domain and the power spectral density (PSD) of the experimental conditions can be estimated. Figure 6 reports the PSD estimates as a function of the waveform frequency and for the two levels of waveform amplitude tested for the Square Wave whilst Figure 7 for the Triangle Wave. The predicted values of the oscillation frequency according to model estimates of Part 1:Analytical modelling are reported as black dashed lines in Figure 6 and Figure 7. The oscillation peaks of the PSD can be clearly identified in correspondence of the theoretical frequency induced over the melt or in multiples or dividers of such frequency.

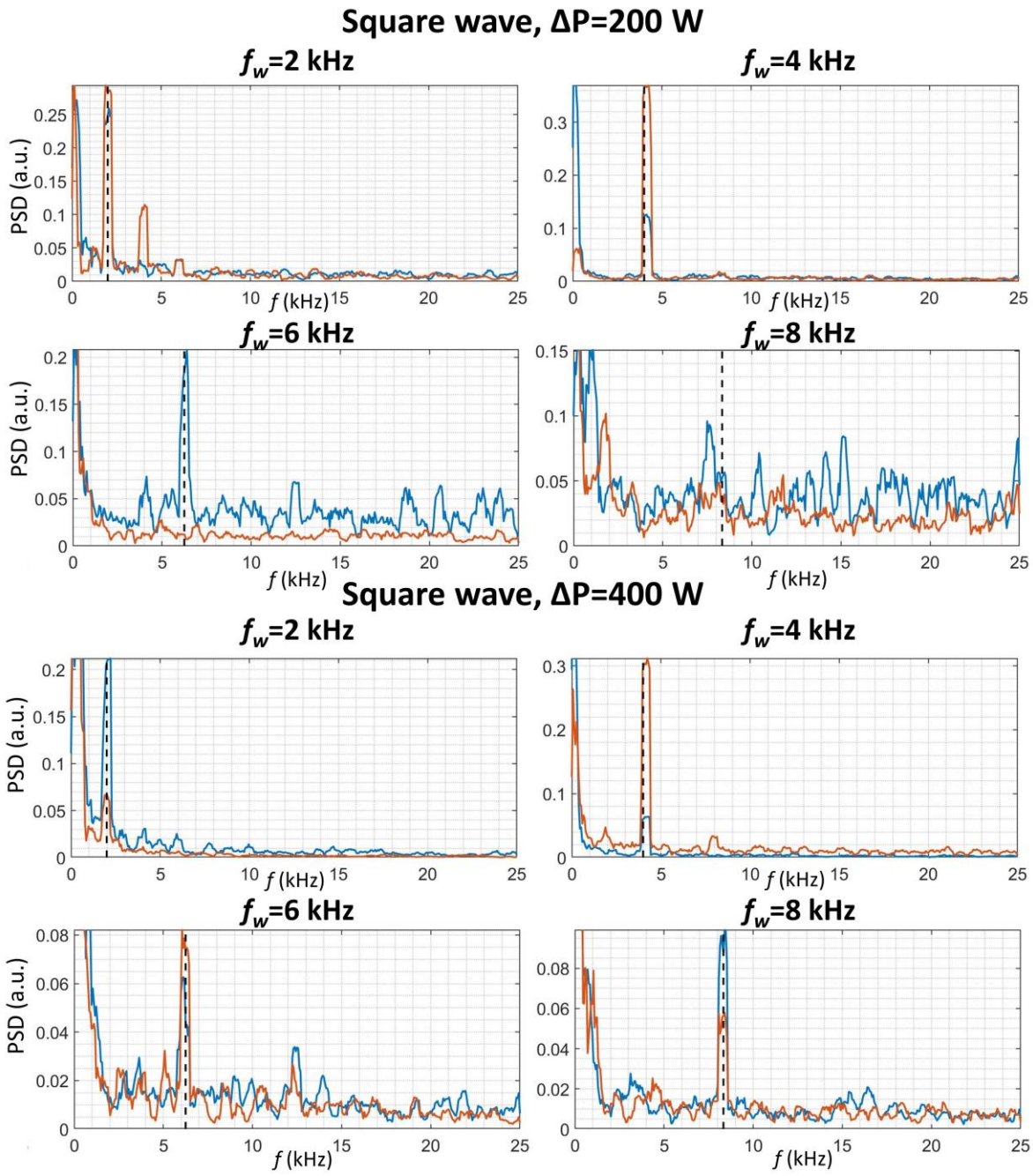

Figure 6. Power Spectral Density estimate of the $I_{sum,ROI}$ indicator for the Square Wave condition which allowed to identify main oscillatory peaks. Black dashed line indicates expected oscillation peak according to analytical model. PSD estimate of replicate 1 and replicate 2 respectively in blue and orange.

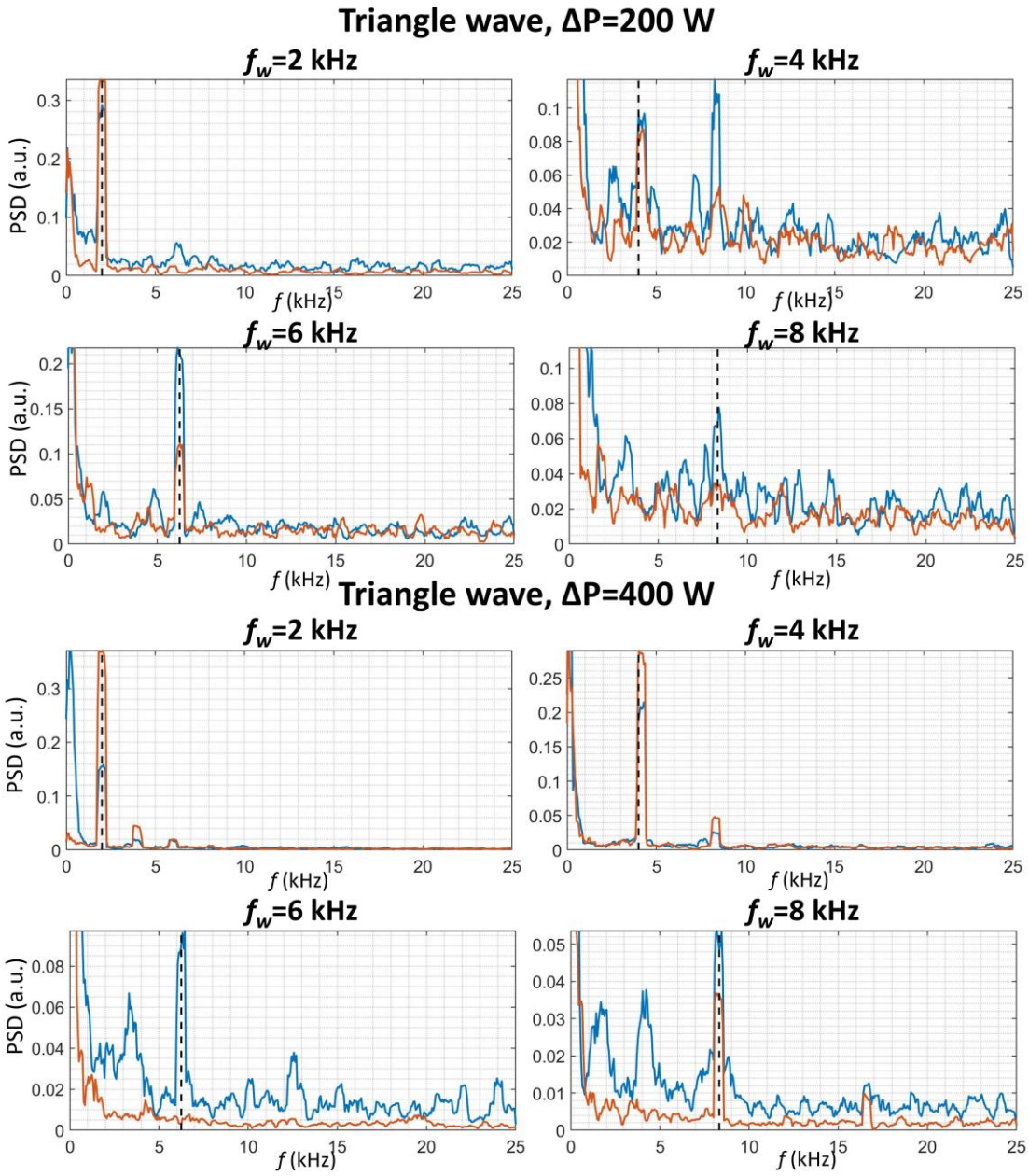

Figure 7. Power Spectral Density estimate of the $I_{sum,ROI}$ indicator for the Triangle Wave condition which allowed to identify main oscillatory peaks. Black dashed line indicates expected oscillation peak according to analytical model. PSD estimate of replicate 1 and replicate 2 respectively in blue and orange.

As predicted in Part I: Analytical modelling of the present work and confirmed by the correspondence between theoretically predicted values and oscillation peaks reported in Figure 6 and Figure 7. The correspondence between imposed frequency and melt oscillations has also been confirmed by Heider *et al.*[35] during the laser welding of Cu alloys. Interestingly enough, the melt oscillation induced over the material occurs independently of the waveform shape employed, as demonstrated in the power spectral density estimates reported in Figure 8 for f_w=2

kHz and with ΔP=200 W. Also in the case of the different waveforms an agreement between the imposed waveform frequency and the oscillatory peaks of the power spectral density may be found.

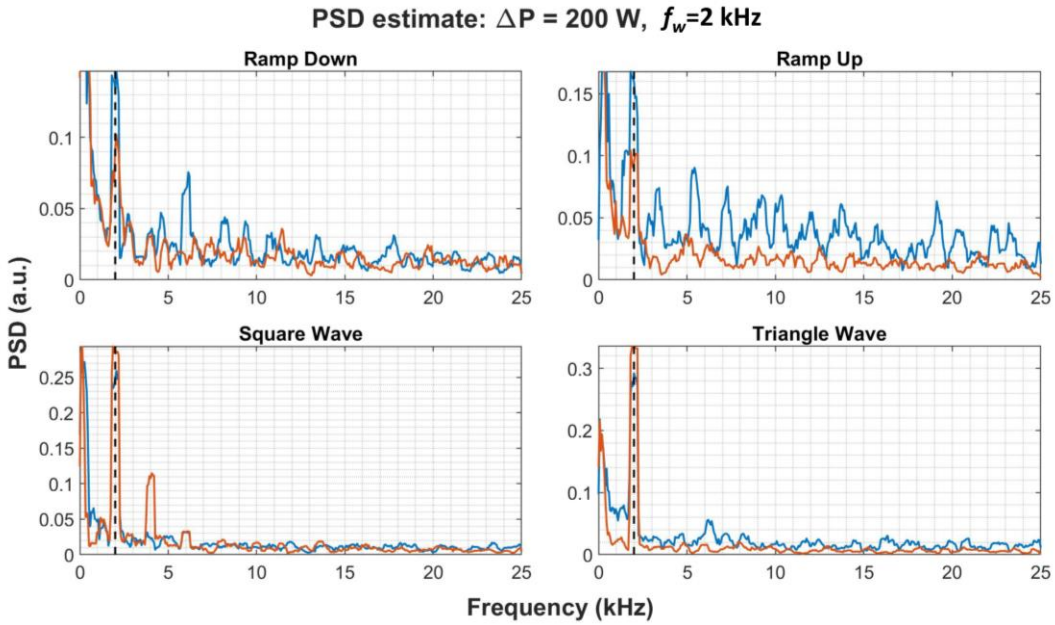

Figure 8. Power Spectral Density estimate of the $I_{sum,ROI}$ indicator which allowed to identify main oscillatory peaks. Black dashed line indicates expected oscillation peak according to analytical model. PSD estimate of replicate 1 and replicate 2 respectively in blue and orange.

3.3 Characterization of single track depositions

Figure 9 shows top view optical microscopy images of the single tracks deposited with the different waveform profiles. The melt dynamics observed via the high speed videography find a correspondence in the consolidated track geometries. Evidently, the conditions which present sudden increases in the temporal profile of the emission power (i.e. Ramp Down and Square waveforms) displayed greater instabilities in the deposition process such as melt ejections and report a discontinuous track formation with the presence of humps similar to balling instability. On the other hand, conditions where a stable melt formation could be denoted in the high speed videos (Ramp Up and Triangle wave) exhibit a continuous seam symptomatic of a stable process. As reported in literature by Yadroitsev *et al.*, these single track deposition conditions should be investigated attentively when moving toward multi-track and multi-layer depositions[36]. Although evidence of stable single track deposition may be considered as the first step towards the development of an additive manufacturing process, when moving towards multi-track and multi-layer processing conditions significant challenges can be expected due to the effect that neighbouring

scan tracks can have. For instance, variations in the melting conditions when moving from the first track to multi-tracks during a single layer deposition have been observed experimentally by Bruna-rosso *et al.*[37]. Further attention towards the deposition of bulk specimen is therefore required to extend the applicability of temporal waveform modulation to multi-track and multi-layer conditions.

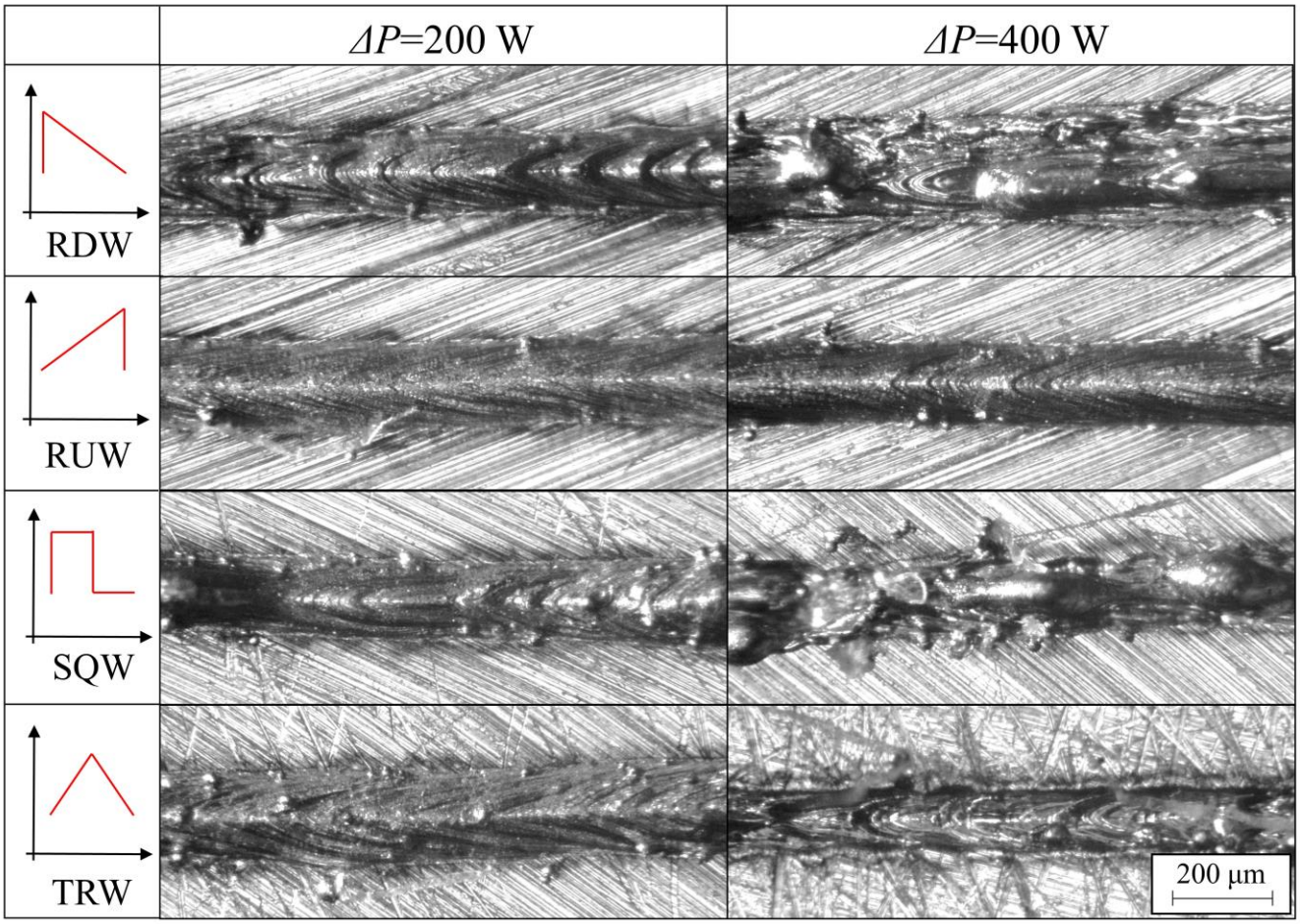

Figure 9. Top view image of the single track depositions obtained with the different waveform shapes and the two levels of waveform amplitude. Images representative of the different frequency levels.

In order to disclose the sub-surface melt geometry, metallographic analysis was conducted on the deposited samples. Figure 10 shows representative conditions for the different waveforms and waveform amplitude tested in the current work. Although the cross-sections have been cut transversally to the laser advancement direction and can thus be considered representative of a instant of the deposition, the . In general, depositions with a lower waveform amplitude (ΔP=200 W) tend to not exhibit pores . Contrarily, at ΔP=400 W, porosity is often found in the single track depositions and a high variability in terms of penetration depth may be observed. The higher

waveform amplitude oscillation in the case of the Square Wave clearly exhibits the morphology of keyhole induced pores which are generated by an elevated level of recoil pressure which enables the a deep penetration within the base material.

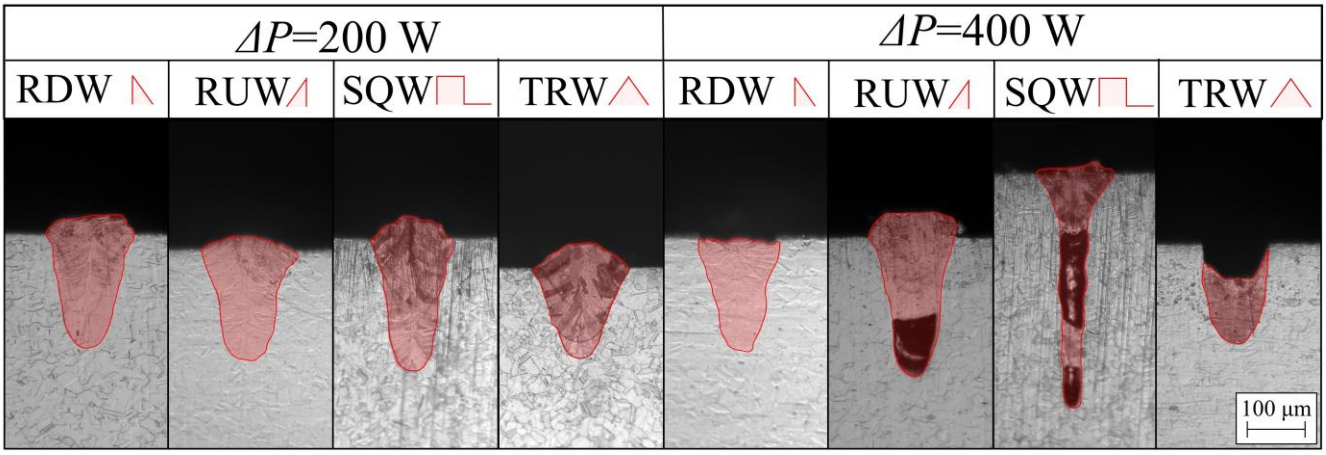

Figure 10. Metallographic cross-sections for the various combination of waveform shapes and wave amplitude *ΔP*. Cross-section representative of the different wave frequency levels.

An important indicator in terms of process stability is the build rate achievable at single track level, reported for the different conditions in Figure 11. This parameter allows to clearly display conditions which enable a stable LPBF process. On the other hand, negative build rates might be of greater interest for material removal processes where waveform modulation can be an useful tool as indicated by Ly *et al.* for the laser drilling process [38]. Waveform shapes with sudden increases of the emission power (i.e. Ramp Down and Square waveforms), appear to be more apt for material removal processes considering the negative build rate reported for such conditions in Figure 11. This aspect thus suggests that rather than employing the conventional Square Wave shape for temporal modulation, gradual ramping of the power emission can avoid generating sudden rises in terms of recoil pressure over the melt surface and with a reduced perturbation of the melt dynamics (as confirmed by the high speed imaging observations previously discussed).

As anticipated by the high speed imaging acquisitions and optical microscopy images, conditions with a large waveform amplitude (*ΔP*=400 W) tend to be detrimental for the deposition process and are generally below the reference level of the CW emission deposition. On the other hand, when the waveform oscillation is limited in terms of magnitude (*ΔP*=200 W) the deposition process stabilizes and values comparable to CW emission are

reported. Once again, the waveform shapes which promote a stable deposition behaviour are Ramp Up and Triangle Wave.

Always analysing the data reported in Figure 11, there appears to be a significant trend, whereby lower levels of waveform frequency tend to promote higher values of build rate. Such effect appears to be most significant in the case of less stable depositions where defects typical of keyhole formation are observable. This aspect may be correlated to the fact that lower levels of waveform frequency, from a single pulse temporal perspective, imply a longer period where the melt is exposed to the higher levels of emission power and consequently greater levels of recoil pressure (in accordance with higher peak temperatures reported in Part I for such conditions). Thus at single plus level, a greater deformation of the melt-surface may be expected possibly modifying the coupling behaviour between the incident laser beam and the melt due to a greater amount of internal reflections. Such effects which imply modifications in the process dynamics have been reported in literature for the keyhole welding [39]. Similar changes have been reported by Cunningham *et al.* at different power levels under CW emission during the LPBF process, but may be expected to occur periodically during time-modulated laser emission[40]. In order, to validate such hypothesis, further investigation are required to analyse the melting front of the keyhole (for instance via X-ray transmission imaging of the process). Nonetheless, the fact that at lower levels a higher build rate is reported is most likely correlated to the coupling efficiency between the laser beam and the underlying material. However, a limiting effect may be expected in employing excessively low modulation frequencies since the process might well revert to surface structuring dynamics as in the work by Temmler *et al.*[41].

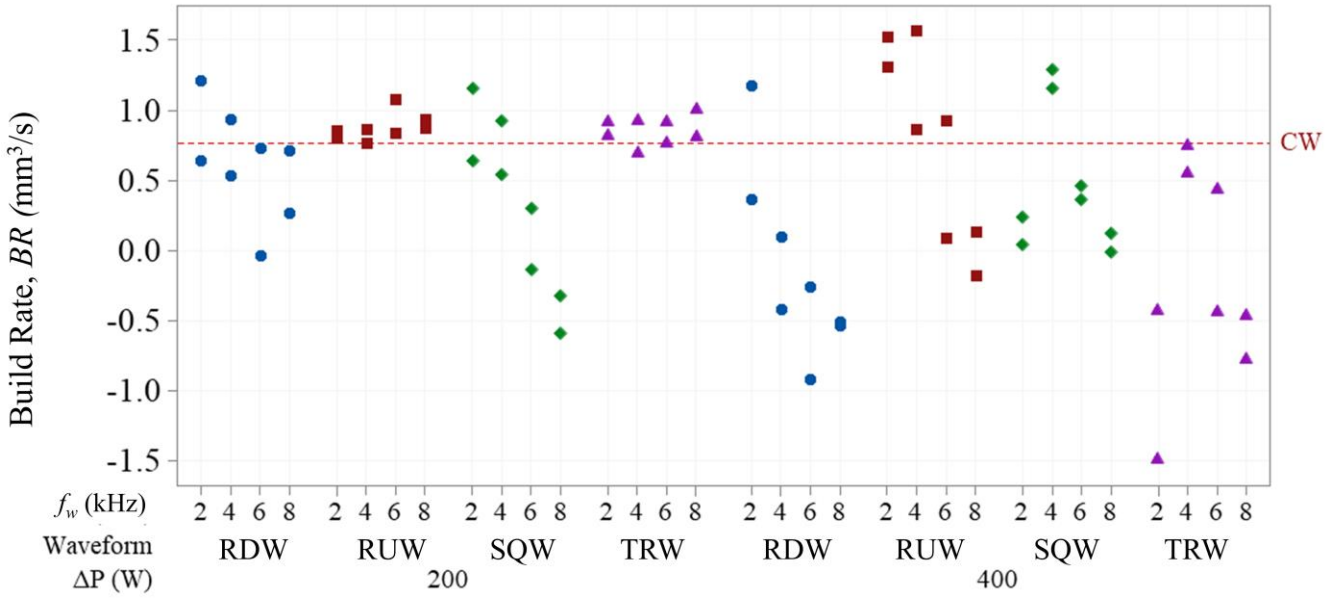

Figure 11. Individual value plot of build rate for each combination of process parameters. Dashed line in red to indicate reference level for CW emission deposition. Error bars reporting measurement variability are not reported due to low standard deviation.

In terms of quality, the single track deposition were characterised by means of roughness which are reported in Figure 12. As a consequence of the instability generated by the excessive power variations, single tracks deposited with large levels of waveform amplitude (ΔP=400 W) yielded inconsistent results with values well beyond the reference level of CW emission. Analogously, the Ramp Down and Square Waveform at ΔP=200 W exhibit high values of roughness. On the other hand, Ramp Up and Triangle Wave deposition appear to be promising candidates, even achieving beneficial effects at single track level with respect to the CW deposition. In such cases, the use of lower waveform oscillation frequencies yielded lower values of roughness. Thus, the use of waveform modulation may be a viable solution to improve the surface finishing of AM produced components.

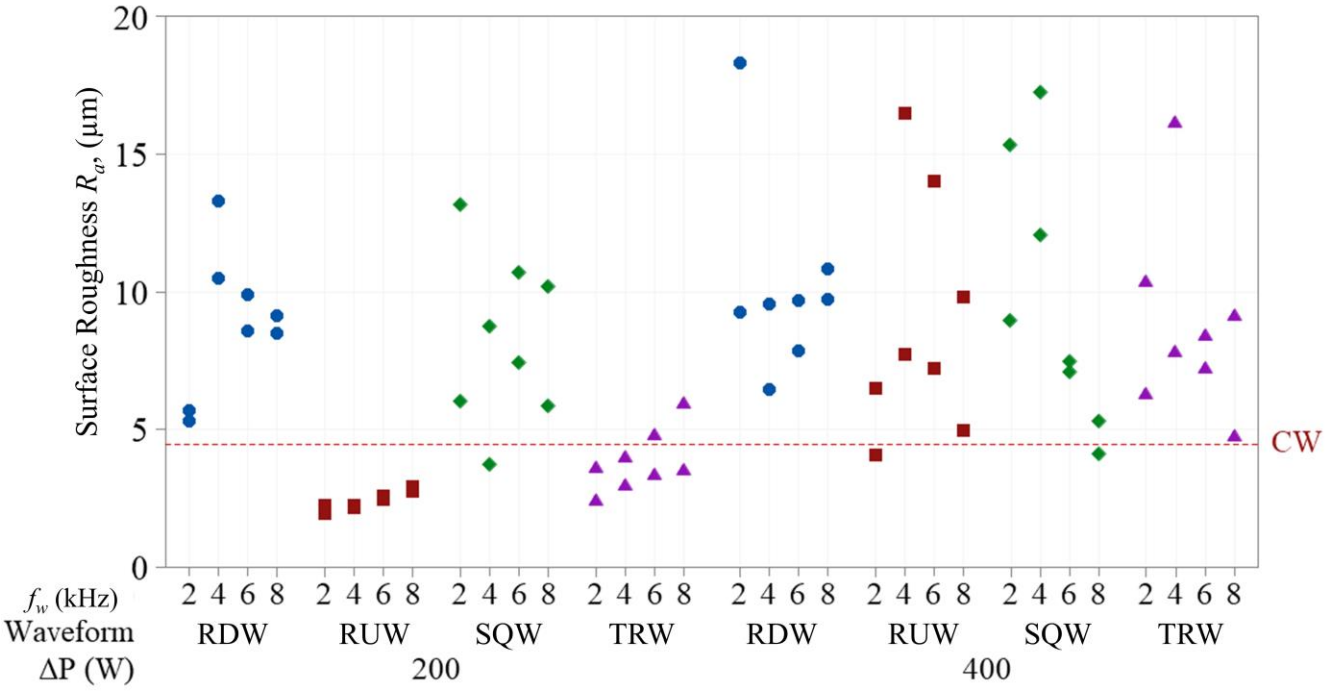

Figure 12. Surface roughness of single track top profile for each combination of process parameters. Dashed line in red to indicate reference level for CW emission deposition. Error bars reporting measurement variability are not reported due to low standard deviation.

4 Discussion

Results of the present work are still preliminary and obtained at single track level which thus implies that further work is required to disclose the effect over multi-track and multi-layer components. Nonetheless, indications towards the appropriate choice of parameters for temporal modulation in the LPBF process has been provided and are in accordance with the theoretical predictions of the analytical model presented in Part I of this work. Beneficial effects appear to be correlated to the surface finishing of the depositions but may also have an impact over the metallurgical aspects. For instance, the possibility of controlling the melt flow and its motion frequency may allow the breaking of dendrites during the rapid solidification process or alter the solidification rates. Similar approaches have been implemented via beam spatial oscillation by Hagenlocher *et al.* and by Wang *et al.* to modify the solidification conditions during the laser welding of crack susceptible Al-alloys [42,43]. Future developments related to a more detailed analysis of the metallurgy of the deposited samples may help disclose such aspects.

Figure 13 reports the mapping of the measured molten pool oscillation frequency against the nominal values in the different experimental conditions (i.e. waveform shape, amplitude and frequency). As reported previously, the oscillation frequency $f_{osc,meas}$ measured via the high speed imaging videos in this work found a strong correspondence to the imposed waveform frequencies f_w.

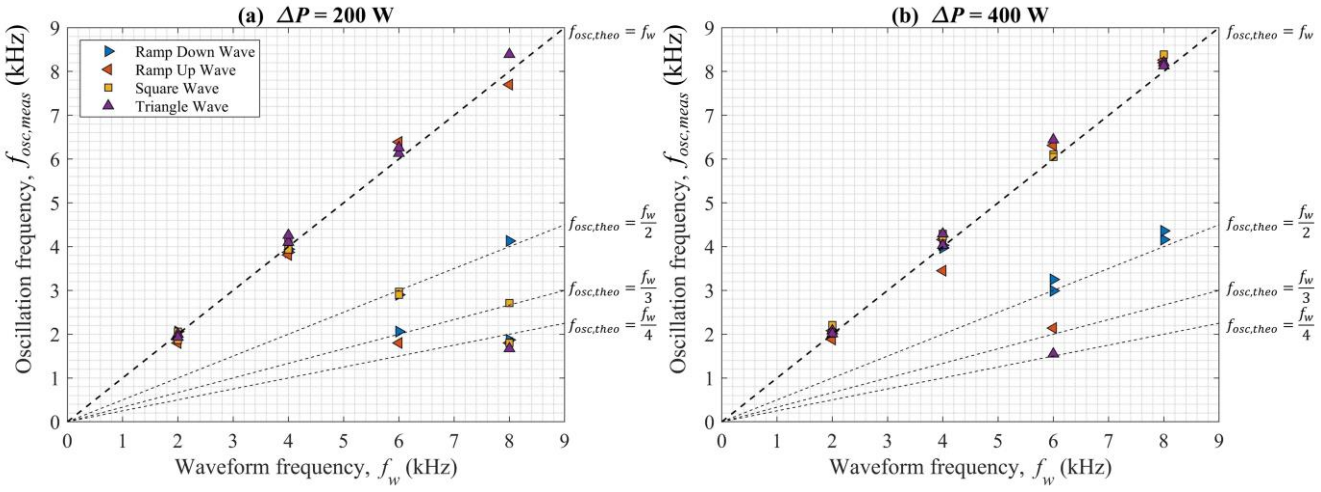

Figure 13. Molten pool oscillation frequency $f_{osc,meas}$ measured via the high speed imaging acquisitions against nominal waveform frequency f_w for experiments at (a) ΔP=200 W and (b) ΔP=400 W. Dashed lines report analytical model prediction for $f_{osc,theo}$

The majority of the measured values of $f_{osc,meas}$ shown in Figure 13 correspond to f_w with a directly proportional relationship confirming the analytical model predictions ($f_{osc,theo} = f_w$). On the other hand, in some cases multiples or submultiples of the frequency are identified via the PSD analysis of the high speed acquisitions. The relationship $f_{osc,theo} = f_w$ is in agreement with the analytical model formulated in Part I of the present work based on the assumption of a linear transfer function between the forcing frequency and the melt pool. However, the fact that the melt pool oscillatory motion evolves towards sub-multiples of the forcing frequency is typical of non-linear systems[44]. This phenomenon can be observed in a pronounced manner at the higher levels of waveform frequency tested in the current experimental campaign independently of the waveform amplitude and shape employed. A non-linear behaviour, as the one denoted at higher levels of waveform frequency (and consequently Simon's number), may be found in a wide variety of physical problems dealing with both mechanical and fluid dynamic aspects of the latter[45,46]. As could be expected, this indicates a complex dynamics associated to the molten pool motion under study which may require more advanced modelling approaches. Computational fluid-

dynamics could be of aid in representing the full complexity of the problem and proposing exact predictions. Still, the analytical modelling proposed in Part I which indicates the recoil pressure as the dominating factor in influencing the molten pool oscillations may be considered valid if we can accept the hypothesis of a linear mechanical system.

The experimental results reported in the present investigation allow to validate the model correlating the melt pool surface motion to a temporally modulated power input for stainless steel AISI316L. Nonetheless, considering that the recoil pressure generation mechanism has been documented for different materials and that analytical model presented in Part I may adapted to consider different thermophysical properties, it is possible to consider that the relationship between laser waveform modulation and melt pool oscillation will be found consistent also for other materials typically processed by LPBF. Clearly, the interaction area and magnitude of the pressure field over the molten pool surface will be strictly regulated by the thermal field generated by the laser material interaction (thus the thermophysical parameters of the material and the energy coupling mechanisms). Still, it is possible to expect that the temporally modulated behaviour will be maintained and that the material oscillatory behaviour will correspond to the input waveform frequency value. Analysing the scientific literature it is possible to observe that the oscillatory behaviour generated by a temporally modulated beam has previously been reported by Stritt *et al.* during the laser welding of Cu[47,48]. Considering the results by Temmler *et al.* on IN718 with waveform modulation of the laser power, it may be expected that such relationship may also be found truthful for Ni-based alloys[41].

A parameter which can be extrapolated from the analytical model of Part I and that governs the thermal field of the process is Simon's number Si which is defined as[49,50]:

$$\mathrm{Si} = \frac{8\pi f_w \alpha}{v^2} \tag{2}$$

where α is the thermal diffusivity. Simon's number represent the ratio between the speed of the thermal waves and the waveform frequency of the heat source employed. Although in the present work this non-dimensional number was varied by modifying the waveform frequency parameter only, the results reported suggests that the ratio

between scan velocity and the waveform frequency is a significant parameter to take into account since it may eventually induce changes in the oscillatory behaviour of the melt. The other parameter which is often employed to characterise the waveform emission spatial behaviour is the spatial wavelength of the process (λ_w) which represents the distance travelled by the laser beam between two successive peaks. Such a parameter is strictly correlated to the definition of Simon's number and is formulated as[22]:

$$\lambda_w = \frac{v}{f_w} \tag{3}$$

Accordingly with observations by Temmler *et al.*, a lower super-position between successive peaks (i.e. a greater λ_w) generates a periodical structuring of the surface which may be beneficial in the case of surface texturing applications whilst it might be detrimental for an additive manufacturing process where stable bead formation is preferred[22]. Thus it may be argued that elevated values of Simon's number may be considered symptomatic of a tendency of the system towards a non-linear dynamical behaviour whereas in the case the waveform frequency results too low, a significant separation between successive peaks in the power emission profile may generate a periodical deposition. Hence, in order to control the molten pool oscillation frequency, a compromise between these two conditions must be sought beyond limiting the amplitude ΔP which has proven detrimental due to the increased melt ejections.

An further point of discussion, is correlated to the hypothesis of the recoil pressure dominating the other dynamical aspects involved (such as viscous forces and Marangoni convection). This consideration is valid in the case of large amplitude forces such as does induced in the conditions tested throughout this work (ΔP=200-400 W) where oscillations could be clearly identified at multiples or submultiples of the imposed waveform frequency. On the other hand, lower amplitude variations of the laser power may be ineffective in modifying the melt flow should the forces generated over the molten liquid be smaller than the other dynamic aspects involved. A valid approach to quantify the recoil pressure exerted may be found in the work by Cullom *et al.* and may be the subject of future activities[51]. The sensing principle employed in the present work effectively allowed the measurement of the oscillation frequency via the PSD estimate of the intensity signal from the high speed videography. However, such

method is not appropriate for a quantitative measurement of the recoil force exerted. Once again, computational fluid-dynamic approaches may provide quantitative estimates of the necessary ΔP to control the oscillatory motion in terms of amplitude.

The results of the present work may be of interest and applicable to different advanced laser manufacturing technologies, ranging from welding to surface structuring or directed energy deposition. Knowledge of the driving relationships regarding the thermal and dynamic phenomena may eventually enable the means to develop novel closed loop control architectures as well as enhance the process development and applicability of laser based manufacturing techniques to crack-susceptible materials. Moreover, such techniques may be implemented in different additive manufacturing processes yielding positive effects in terms of resolution and metallurgical features. Evidence of modulated emission impacting the metallurgical features of Laser Metal Deposition has been reported by Xiao *et al.*[18,52]. In general, further studies aimed at investigating the material metallurgy with the the proposed temporal waveforms may also be of interest.

5 Conclusions

The present work demonstrates that the use of temporal waveform modulation of the laser power during the LPBF process effectively modifies the melt flow. The analytical model developed in Part I of the present research which correlated the temperature field generated by the laser beam to the recoil pressure induced over the melt surface thus generating variations in the melt flow has been validated. The melt oscillation frequencies measured from the high speed videography of the process in the different conditions are well in agreement with the theoretical predictions of the analytical model. The experimental investigation also provides the design cues for future experimental design by outlining the effect of different temporal modulation parameters and waveform shapes over the solidification process.

In terms of waveform shapes, rapid rising profiles of the power emission induced significant disturbances over the melt causing the formation of defects and melt ejections. The most promising waveforms for LPBF depositions

resulted being the Ramp Up and the Triangle Wave whereas Ramp Down and Square Wave emission are more prone to process instabilities.

Waveform amplitude should be restrained in order to avoid excessive variations in terms of recoil pressure which can causes process instabilities such as melt ejections or the formation of keyhole pores. Limited oscillations around the average emission power showed to be more effective in inducing melt oscillations whilst maintaining process stability conditions.

Waveform frequency has a second order effect over the melt dynamics and solidification behaviour observable via the high speed videos, although there is a tendency to induce lower order harmonics in the melt flow at high levels of f_w. This is a behaviour symptomatic of a non-linear mechanical system. On the other hand, lower roughness can be achieved if lower levels of waveform frequency are employed.

Build rate achievable in stable conditions with waveform modulation are comparable to values obtainable with continuous wave emission. Moreover, at single track deposition level, the use temporal profiles of the power emission appears to have a beneficial effect over the roughness.

The possibility of modifying the molten pool oscillatory motion by modulating the laser emission power may impact significantly the metallurgical aspects of the material, thus future investigations will study such aspects in a detail. Moreover, the tools developed in the present work for the LPBF technology may be applied transversally to different laser manufacturing technologies.

Acknowledgements

The authors gratefully acknowledge the BLM Group for providing the high-speed imaging hardware. Optoprim Srl and nLight Inc are acknowledged for providing the laser and optical chain. The Italian Ministry of Education, University and Research is acknowledged for the support provided through the Project "Department of Excellence LIS4.0 - Lightweight and Smart Structures for Industry 4.0". Tommaso Corti is acknowledged for the support provided throughout the experimental activities.

References

[1] M. Schmidt, M. Merklein, D. Bourell, D. Dimitrov, T. Hausotte, K. Wegener, L. Overmeyer, F. Vollertsen, G.N. Levy, Laser based additive manufacturing in industry and academia, CIRP Ann. 66 (2017) 561–583. https://doi.org/10.1016/j.cirp.2017.05.011.

[2] A.G. Demir, P. Colombo, B. Previtali, From pulsed to continuous wave emission in SLM with contemporary fiber laser sources: effect of temporal and spatial pulse overlap in part quality, Int. J. Adv. Manuf. Technol. 91 (2017) 2701–2714. https://doi.org/10.1007/s00170-016-9948-7.

[3] L. Caprio, A.G. Demir, B. Previtali, Influence of pulsed and continuous wave emission on melting efficiency in selective laser melting, J. Mater. Process. Technol. 266 (2019) 429–441. https://doi.org/10.1016/j.jmatprotec.2018.11.019.

[4] A. V. Gusarov, S.N. Grigoriev, M.A. Volosova, Y.A. Melnik, A. Laskin, D. V. Kotoban, A.A. Okunkova, On productivity of laser additive manufacturing, J. Mater. Process. Technol. 261 (2018) 213–232. https://doi.org/10.1016/j.jmatprotec.2018.05.033.

[5] T.T. Roehling, S.S.Q. Wu, S.A. Khairallah, J.D. Roehling, S.S. Soezeri, M.F. Crumb, M.J. Matthews, Modulating laser intensity profile ellipticity for microstructural control during metal additive manufacturing, Acta Mater. 128 (2017) 197–206. https://doi.org/10.1016/j.actamat.2017.02.025.

[6] R. Shi, S.A. Khairallah, T.T. Roehling, T.W. Heo, J.T. McKeown, M.J. Matthews, Microstructural control in metal laser powder bed fusion additive manufacturing using laser beam shaping strategy, Acta Mater. 184 (2020) 284–305. https://doi.org/10.1016/j.actamat.2019.11.053.

[7] C. Tenbrock, F.G. Fischer, K. Wissenbach, J.H. Schleifenbaum, P. Wagenblast, W. Meiners, J. Wagner, Influence of keyhole and conduction mode melting for top-hat shaped beam profiles in laser powder bed fusion, J. Mater. Process. Technol. 278 (2020) 116514. https://doi.org/10.1016/j.jmatprotec.2019.116514.

[8] M. Cloots, P.J. Uggowitzer, K. Wegener, Investigations on the microstructure and crack formation of IN738LC samples processed by selective laser melting using Gaussian and doughnut profiles, Mater. Des. 89 (2016) 770–784. https://doi.org/10.1016/j.matdes.2015.10.027.

[9] M. Zavala-Arredondo, N. Boone, J. Willmott, D.T.D. Childs, P. Ivanov, K.M. Groom, K. Mumtaz, Laser diode area melting for high speed additive manufacturing of metallic components, Mater. Des. 117 (2017) 305–315. https://doi.org/10.1016/j.matdes.2016.12.095.

[10] W. Zhang, W. Hou, L. Deike, C.B. Arnold, Using a dual-laser system to create periodic coalescence in laser powder bed fusion, Acta Mater. 201 (2020) 14–22. https://doi.org/10.1016/j.actamat.2020.09.071.

[11] T. Heeling, K. Wegener, The effect of multi-beam strategies on selective laser melting of stainless, Addit. Manuf. 22 (2018) 334–342. https://doi.org/10.1016/j.addma.2018.05.026.

[12] M.J. Matthews, G. Guss, D.R. Drachenberg, J.A. Demuth, J.E. Heebner, E.B. Duoss, J.D. Kuntz, C.M. Spadaccini, Diode-based additive manufacturing of metals using an optically-addressable light valve, Opt. Express. 25 (2017) 11788. https://doi.org/10.1364/OE.25.011788.

[13] K.A. Mumtaz, N. Hopkinson, Selective Laser Melting of thin wall parts using pulse shaping, J. Mater. Process. Technol. 210 (2010) 279–287. https://doi.org/10.1016/j.jmatprotec.2009.09.011.

[14] L. Caprio, A.G. Demir, B. Previtali, Comparative study between CW and PW emissions in selective laser melting, J. Laser Appl. 30 (2018) 32305. https://doi.org/10.2351/1.5040631.

[15] A.G. Demir, L. Mazzoleni, L. Caprio, M. Pacher, B. Previtali, Complementary use of pulsed and continuous wave emission modes to stabilize melt pool geometry in laser powder bed fusion, Opt. Laser Technol. 113 (2019). https://doi.org/10.1016/j.optlastec.2018.12.005.

[16] C.A. Biffi, J. Fiocchi, P. Bassani, A. Tuissi, Continuous wave vs pulsed wave laser emission in selective laser melting of AlSi10Mg parts with industrial optimized process parameters: microstructure and

mechanical behaviour, Addit. Manuf. 24 (2018) 639–646. https://doi.org/10.1016/j.addma.2018.10.021.

[17] A.E. Wilson-Heid, Z. Wang, B. McCornac, A.M. Beese, Quantitative relationship between anisotropic strain to failure and grain morphology in additively manufactured Ti-6Al-4V, Mater. Sci. Eng. A. 706 (2017) 287–294. https://doi.org/10.1016/j.msea.2017.09.017.

[18] H. Xiao, S. Li, X. Han, J. Mazumder, L. Song, Laves phase control of Inconel 718 alloy using quasi-continuous-wave laser additive manufacturing, Mater. Des. 122 (2017) 330–339. https://doi.org/10.1016/j.matdes.2017.03.004.

[19] H. Xiao, P. Xie, M. Cheng, L. Song, Enhancing mechanical properties of quasi-continuous-wave laser additive manufactured Inconel 718 through controlling the niobium-rich precipitates, Addit. Manuf. 34 (2020) 101278. https://doi.org/10.1016/j.addma.2020.101278.

[20] S. Baraldo, A. Vandone, A. Valente, E. Carpanzano, Closed-loop control by laser power modulation in direct energy deposition additive manufacturing, in: Proc. 5th Int. Conf. Ind. 4.0 Model Adv. Manuf., 2020: pp. 129–143.

[21] F.C. Neto, M.C. Fredel, M. Pereira, L.E. dos S. Paes, Laser power modulation to grain refinement of SAE 1045 steel welds, J. Laser Appl. 32 (2020) 022027. https://doi.org/10.2351/7.0000096.

[22] A. Temmler, D. Wei, T. Schmickler, M.E. Küpper, C.L. Häfner, Experimental investigation on surface structuring by laser remelting (WaveShape) on Inconel 718 using varying laser beam diameters and scan speeds, Appl. Surf. Sci. 541 (2021) 147814. https://doi.org/10.1016/j.apsusc.2020.147814.

[23] J. Ning, L.J. Zhang, L. liang Zhang, J. Long, X. qing Yin, J.X. Zhang, S.J. Na, Effects of power modulation on behaviours of molten pool and keyhole during laser–arc hybrid welding of pure copper, Mater. Des. 194 (2020) 108829. https://doi.org/10.1016/j.matdes.2020.108829.

[24] J. Ning, S.J. Na, L.J. Zhang, X. Wang, J. Long, W.I. Cho, Improving thermal efficiency and stability of

laser welding process for magnesium alloy by combining power modulation and subatmospheric pressure environment, J. Magnes. Alloy. (2021). https://doi.org/10.1016/j.jma.2021.02.005.

[25] L. Caprio, A.G. Demir, B. Previtali, Non-intrusive estimation of subsurface geometrical attributes of the melt pool through the sensing of surface oscillations in laser powder bed fusion, J. Laser Appl. 33 (2020) 12035. https://doi.org/10.2351/7.0000323.

[26] L. Caprio, A.G. Demir, B. Previtali, B.M. Colosimo, Determining the feasible conditions for processing lunar regolith simulant via Laser Powder Bed Fusion, Addit. Manuf. 32 (2020) 101029. https://doi.org/https://doi.org/10.1016/j.addma.2019.101029.

[27] B. Ferrar, L. Mullen, E. Jones, R. Stamp, C.J. Sutcliffe, Gas flow effects on selective laser melting (SLM) manufacturing performance, J. Mater. Process. Technol. 212 (2012) 355–364. https://doi.org/10.1016/j.jmatprotec.2011.09.020.

[28] S. Zhao, L. Yang, T. Liu, R. Yang, J. Pan, Analysis of plasma oscillations by electrical detection in Nd:YAG laser welding, J. Mater. Process. Technol. 249 (2017) 479–489. https://doi.org/10.1016/j.jmatprotec.2017.06.032.

[29] Y. Chen, P. Wen, M. Voshage, L. Jauer, Y. Qin, J.H. Schleifenbaum, R. Poprawe, Laser additive manufacturing of Zn metal parts for biodegradable implants: Effect of gas flow on evaporation and formation quality, J. Laser Appl. 31 (2019) 022304. https://doi.org/10.2351/1.5096118.

[30] L. Mazzoleni, A.G. Demir, L. Caprio, M. Pacher, B. Previtali, Real-Time Observation of Melt Pool in Selective Laser Melting: Spatial, Temporal and Wavelength Resolution Criteria, IEEE Trans. Instrum. Meas. 69 (2019) 1179–1190.

[31] L. Caprio, A.G. Demir, B. Previtali, Observing molten pool surface oscillations during keyhole processing in laser powder bed fusion as a novel method to estimate the penetration depth, Addit. Manuf. 36 (2020) 101470. https://doi.org/10.1016/j.addma.2020.101470.

[32] I. Yadroitsev, A. Gusarov, I. Yadroitsava, I. Smurov, Single track formation in selective laser melting of metal powders, J. Mater. Process. Technol. 210 (2010) 1624–1631. https://doi.org/10.1016/j.jmatprotec.2010.05.010.

[33] Y. Wang, L. Xing, K. Li, C. Yu, J. Ma, W. Liu, Z. Shen, Band-Like Distribution of Grains in Selective Laser Melting Track Under Keyhole Mode, Metall. Mater. Trans. B Process Metall. Mater. Process. Sci. 50 (2019) 1035–1041. https://doi.org/10.1007/s11663-018-1483-5.

[34] V. V Semak, J.A. Hopkins, M.H. Mccay, T.D. Mccay, A concept for a hydrodynamic model of keyhole formation and support during laser welding, in: Int. Congr. Appl. Lasers Electro-Optics, 1994: pp. 641–650. https://doi.org/10.2351/1.5058848.

[35] A. Heider, A. Hess, R. Weber, T. Graf, Stabilized copper welding by using power modulated green and ir laser beams, 30th Int. Congr. Appl. Lasers Electro-Optics, ICALEO 2011. 395 (2011) 395–402. https://doi.org/10.2351/1.5062263.

[36] I. Yadroitsev, P. Krakhmalev, I. Yadroitsava, Hierarchical design principles of selective laser melting for high quality metallic objects, Addit. Manuf. 7 (2015) 45–56. https://doi.org/10.1016/j.addma.2014.12.007.

[37] C. Bruna-rosso, A.G. Demir, B. Previtali, Selective laser melting finite element modeling : Validation with high-speed imaging and lack of fusion defects prediction, Mater. Des. 156 (2018) 143–153. https://doi.org/10.1016/j.matdes.2018.06.037.

[38] S. Ly, G. Guss, A.M. Rubenchik, W.J. Keller, N. Shen, R.A. Negres, J. Bude, Resonance excitation of surface capillary waves to enhance material removal for laser material processing, Sci. Rep. 9 (2019) 1–9. https://doi.org/10.1038/s41598-019-44577-6.

[39] R. Fabbro, Melt pool and keyhole behaviour analysis for deep penetration laser welding, J. Phys. D. Appl. Phys. 43 (2010) 445501. https://doi.org/10.1088/0022-3727/43/44/445501.

[40] R. Cunningham, C. Zhao, N. Parab, C. Kantzos, J. Pauza, K. Fezzaa, T. Sun, A.D. Rollett, Keyhole threshold and morphology in laser melting revealed by ultrahigh-speed x-ray imaging, Science (80-.). 363 (2019) 849–852. https://doi.org/10.1126/science.aav4687.

[41] A. Temmler, N. Pirch, J. Luo, J.H. Schleifenbaum, C.L. Häfner, Numerical and experimental investigation on formation of surface structures in laser remelting for additive-manufactured Inconel 718, Surf. Coatings Technol. 403 (2020) 126370. https://doi.org/10.1016/j.surfcoat.2020.126370.

[42] C. Hagenlocher, M. Sommer, F. Fetzer, R. Weber, T. Graf, Optimization of the solidification conditions by means of beam oscillation during laser beam welding of aluminum, Mater. Des. 160 (2018) 1178–1185. https://doi.org/10.1016/j.matdes.2018.11.009.

[43] L. Wang, M. Gao, C. Zhang, X. Zeng, Effect of beam oscillating pattern on weld characterization of laser welding of AA6061-T6 aluminum alloy, Mater. Des. 108 (2016) 707–717. https://doi.org/10.1016/j.matdes.2016.07.053.

[44] J.A. Rooney, Nonlinear phenomena, Methods Exp. Phys. 19 (1981) 299–353. https://doi.org/10.1016/S0076-695X(08)60337-3.

[45] D.B. Blocher, A.T. Zehnder, R.H. Rand, Entrainment of micromechanical limit cycle oscillators in the presence of frequency instability, J. Microelectromechanical Syst. 22 (2013) 835–845. https://doi.org/10.1109/JMEMS.2013.2248124.

[46] S.J. Baek, S.B. Lee, H.J. Sung, Response of a circular cylinder wake to superharmonic excitation, J. Fluid Mech. 442 (2001) 67–88. https://doi.org/10.1017/S0022112001004980.

[47] M. Jarwitz, F. Fetzer, P. Stritt, R. Weber, T. Graf, Influence of laser power modulation on the time-resolved temperature distribution in the weld pool during laser welding of copper to aluminum, Lasers Manuf. Conf. 2015 Influ. (2015).

[48] P. Stritt, R. Weber, T. Graf, S. Müller, C. Ebert, Utilizing laser power modulation to investigate the transition from heat-conduction to deep-penetration welding, Phys. Procedia. 12 (2011) 224–231. https://doi.org/10.1016/j.phpro.2011.03.029.

[49] J.M. Dowden, The mathematics of thermal modeling: an introduction to the theory of laser material processing, CRC Press, 2001.

[50] G. Simon, U. Gratzke, J. Kroos, Analysis of heat conduction in deep penetration welding with a time-modulated laser beam, J. Phys. D. Appl. Phys. 26 (1993) 862–869. https://doi.org/10.1088/0022-3727/26/5/022.

[51] T. Cullom, C. Lough, N. Altese, D. Bristow, R. Landers, B. Brown, T. Hartwig, A. Barnard, J. Blough, K. Johnson, E. Kinzel, Frequency domain measurements of melt pool recoil force using modal analysis, Sci. Rep. 11 (2021) 1–12. https://doi.org/10.1038/s41598-021-90423-z.

[52] S. Li, H. Xiao, K. Liu, W. Xiao, Y. Li, X. Han, J. Mazumder, L. Song, Melt-pool motion, temperature variation and dendritic morphology of Inconel 718 during pulsed- and continuous-wave laser additive manufacturing: A comparative study, Mater. Des. 119 (2017) 351–360. https://doi.org/10.1016/j.matdes.2017.01.065.

List of tables

List of figures